ONBOARD IMAGE PROCESSING FOR AUTONOMOUS SPACECRAFT DETECTION OF VOLCANIC PLUMES. D. R. Thompson[1,2], M. Bunte[3], R. Castaño[1], S. Chien[1], R. Greeley[3], [1]Jet Propulsion Laboratory, California Institute of Technology, 4800 Oak Grove Dr., Pasadena, CA 91109, [2]david.r.thompson@jpl.nasa.gov, [3]School of Earth and Space Exploration, Arizona State University.

Introduction: Outer planets missions have imaged active volcanic plumes at Io and Enceladus. These phenomena provide key constraints on subsurface processes and models of planetary composition [1]. To date, over 70 distinct images containing plumes have been collected. Since these plumes are transient events and cannot be anticipated in advance, capturing them requires good luck and many images. This demands a prohibitive fraction of the spacecraft's limited cache and bandwidth, and generally precludes surveys dedicated to monitoring plume activity.

Onboard processing could enable long-term plume monitoring campaigns that use very high rates of image capture. The spacecraft could search these images onboard for plumes and only save the fraction containing key events for downlink. Similar technologies have recently been demonstrated for change detection on the WATCH system aboard the Mars Exploration Rovers [2]. Here, automated processing identified images containing dust devils. Candidate image regions were enclosed in "subframe" images for preferential transmission. Similar selective downlink strategies could enable plume surveys, with event detections triggering preferential storage and transmission of coincident observations by Thermal or Visible Near-Infrared imagers. In prior research, Bue et al. demonstrate an efficient plume detection algorithm [3]. This research expands on their work with a new algorithm variant (Figure 1) that shows strong performance on a test set of plume images from Enceladus and Io.

Approach: We first analyze the image with the Canny edge detection algorithm [4] to identify the planetary horizon. We then fit an ellipse to the horizon using a RANSAC method [5] that samples random subsets of 6 edge points and computes the optimal interpolating ellipse using the closed-form solution of [6]. The RANSAC algorithm fits several thousand ellipses to random point subsets, scoring each according to the number of total edge pixels that lie within a small distance of this contour. We take the best-fitting ellipse as the horizon.

Next we identify bright pixel regions that lie outside the horizon ellipse. We look for plumes in pixels at altitudes up to a user-defined range of the limb (in this work we use altitudes up to 10% of the planetary diameter). The set of all pixels in this annular region are taken to be the "background;" any with intensity greater than τ standard deviations above the mean are detected as plumes and grouped into contiguous connected regions. For this work, we favor $\tau = 5.0$ as our threshold; more lenient values would result in higher detection rates at the risk of false positive detections.

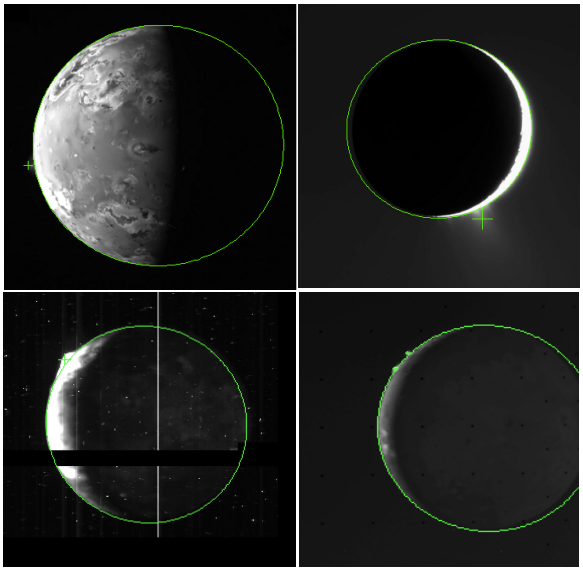

Figure 1: Typical detections. Clockwise from upper left: Galileo 3178r, PIA12733 (excluded from performance analysis), 5147r, Cassini C2066854

A final rule-based filtering step removes detections of unacceptable size and shape: we exclude any region smaller than 5 pixels, with a major axis larger than the planetary radius, or with an extremely eccentric aspect ratio (>5:1) that is characteristic of image streaks due to reflective clutter.

Evaluation: We evaluated the efficacy of plume detection on 19 sequences of single-band images of Io and Enceladus. The images were taken by Galileo and Cassini spacecraft; each sequence contained one or more raw images that had been taken in near succession. Our test set consists of images containing at least half of the planetary disk. Figure 1 shows an example of typical detections from the dataset. A green line follows the best-fit ellipse, and a "plus" shows the size and location of each detected plume. Image 3178r illustrates a small plume on the limb of Io. Image 5147r succeeds despite significant noise and image artifacts. Image C2066854 contains multiple plumes which are successfully detected as independent events. Image PIA12733 is shown as an example Enceladus detection, but it has undergone manual postprocessing so we exclude it from the performance analysis that follows.

Figure 2 shows typical failure cases. Errors in estimating the planetary disk can occur if image quality is poor or the limb is comprised of just a few pixels. Poorly-illuminated plumes occasionally fail to exceed the 5σ detection threshold.

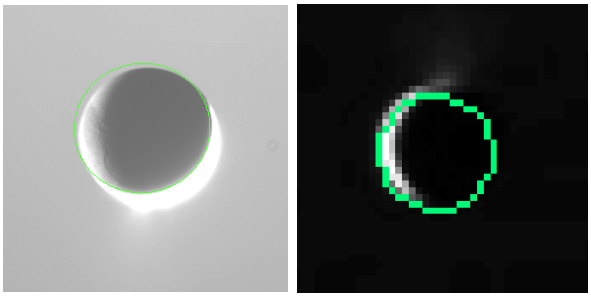

Figure 2: Typical Failure Cases. Left: Cassini N1487335287, where glare and low SNR causes an incorrect disk fit. Right: W00065133, a widefield image with insufficient pixels to identify the limb.

Results: Table 1 below gives performance details. Columns show (Left to Right): a sequence identifier; the number of images; the number of distinct plume events detected; the number of sequence images containing a detection; and specific notes about image quality. There were no false detections in any of the 68 images. Of all sequences containing plumes, 76.9% generated some detection. Those sequences for which detection failed entirely generally suffered from artifacts or poor image quality (Figure 2). 11 distinct plumes were detected out of 19 total. These tests suggest that image quality is a primary constraint on plume detection performance with this algorithm, and that horizon-based approaches are a promising strategy for plume monitoring during a JEO tour phase. A spacecraft system could incorporate onboard ephemeris information for further improvements in both efficiency and detection accuracy.

Acknolwedgements: This research was performed at the Jet Propulsion Laboratory, California Institute of Technology. We thank Brian Bue and Kiri Wagstaff for invaluable assistance.

References: [1] Porco, C., Helfenstein, P., Thomas, P., et al, "Cassini Observes the Active South Pole of Enceladus", *Science*, 311, 1393-1401, 2006 [2] A. Castaño et al., "Automatic detection of dust devils and clouds on Mars," Machine Vision and Applications 19 (6), 2008. [3] B. Bue, K. Wagstaff, R. Castaño, A. Davies. "Automatic Onboard Detection of Planetary Volcanism from Images." LPSC XXXVII Abstract 1717 (2007). [4] J. Canny, in *Readings in computer vision: issues, problems, principles, and paradigms*, 1987. [5] M. A. Fischler, R. C. Bolles, "Random Sample Consensus," Comm. of the ACM, Vol 24, pp 381-395, 1981. [6] A. Fitzgibbon, M. Pilu, and R.B. Fisher, "Direct Least Squares Fitting of Ellipses." *Pattern Analysis and Machine Intelligence,* Vol. 21 No. 5 (1999).

Sequence (Target)	Images	Plumes Detected / Total	# Detection Images	Notes
0085r (Io)	1	1/2	1/1	Missed plume is 2 pixels in altitude
2445r (Io)	1	-	-	
3178r (Io)	1	1/1	-	
320Xr (Io)	3	1/1	3/3	
3485r (Io)	1	1/1	1/1	
4207r (Io)	2	-	-	
5045r-5123r (Io)	3	1/1	3/3	
5147 (Io)	1	1/1	1/1	Imaging artifacts
5407 (Io)	1	1/1	1/1	
554x (Io)	2	1/1	2/2	Imaging artifacts
6300r (Io)	1	-	-	Imaging artifacts
8XXXr (Io)	3	-	-	Plume ambiguous
C2064X (Io)	2	-	-	
C2065X (Io)	2	-	-	
C2066X (Io)	18	2/2	2/18	Very faint plumes
N00015-N00016X (Enc)	3	1/1	1/3	
N148733X (Enc)	19	0/2	0/2	Plume images have low contrast (see Fig. 2)
W0006513 (Enc)	2	0/2	0/2	Target diameter < 40px (see Fig. 2)
W0006514 (Enc)	2	0/3	0/2	Imaging artifacts

Table 1: Detection Performance. No false detections were triggered from this dataset.